Adsorption of Methylene Blue by Hydroxyl-Aluminum Pillared Montmorillonite

[1]Houria Rezala*, [1]Houda Douba, [1]Horiya Boukhatem and [2]Amaya Romero
[1]Université Djilali Bounaama de Khemis-Miliana, Faculté des Sciences et de la Technologie, Route de Thenia El Had, 44001 Khemis-Miliana, Algérie.
[2]Departamento de Ingenieria Quimica, Facultad de Quimicas, Universidad de Castilla-la Mancha, Campus Universitario s/n, 13004 Ciudad Real, Spain.
rezala_houria@hotmail.com*

Summary: A purified raw montmorillonite and hydroxy-aluminum pillared montmorillonite have been prepared from a natural bentonite from Maghnia, Algeria. These materials have been analyzed by X-ray fluorescence spectroscopy, X-ray diffraction, Infrared spectroscopy and nitrogen adsorption-desorption measurement. The pillared montmorillonite provided a certain increase of interlayer basal spacing and BET surface area and consequently the improvement of its capacities adsorption and decolorization of Methylene Blue. The adsorption properties of these materials were studied as a function of contact time, solution pH, initial Methylene Blue concentration and temperature. The adsorption kinetics and isotherms were well fitted by pseudo-second order and Freundlich models, respectively. In addition to that, thermodynamic studies showed an exothermic and a spontaneous process.

Keywords: Methylene blue; Hydroxyl-aluminum pillared montmorillonite; Adsorption; Waste water; Pollution.

Introduction

Organic dyes play important role in various applications. Synthetic Organic dyes discharges pose a great problem for the environment and human health as these latter are generally non-biodegradable [1-3]. Among different types of dyes, Methylene blue (MB) is a basic dye having many uses such as dyeing industry [4]. MB discharges in water lead to disagreeable color and consequently decrease sunlight penetration [5]. MB can cause some harmful effects on the human health such as eye burns, convulsions, and skin irritation. Moreover, it has thermal and light stabilities, complex structure, and low biodegradability [6]. In that regards, it was necessary to treat the MB effluents before throwing in aquatic environment.

Various methods were used for wastewater treatment including chemical [7], biological [8], advanced oxidation process [9] and physical [10, 11]. Among these methods, adsorption remains a relatively used technique and easily to implement because its availability, low cost, and high efficiency [12, 13]. In recent years, there are many research focus on developing new adsorbents for efficient removal of MB from aqueous solution such as graphene oxide [14-18], nanotubes [19], nanocomposite [20-22], metal oxide [23-25], bioadsorbents [26–29], and activated carbon [4, 30-33]. Activated carbon has been the most widely used because of its high adsorption capacity of organic matter. Nevertheless, this adsorbent has a higher cost and remains difficult to regenerate [34]. The search of another effective and less expensive adsorbent is therefore interesting. In this context, the use of clay materials is of great interest because of its low cost, abundance in nature and effectiveness [35].

Clays materials are classified in various types such as kaolinites, palygorskites, chlorites, and smectites [36]. Montmorillonite belongs to smectite and has been widely studied for its capacity to adsorb synthetic dyes [37-44]. However, raw bentonites usually exhibit small surface area due to the strong restack of layers, limiting their applications in dye removal [45]. The inorganic cations (e.g., Na^+ and Ca^{2+}) can be replaced with cationic surfactants or polycationic species, and the resulting materials are regarded as organobentonite or pillared bentonite, respectively [46].

Various hydroxymetal polycations have been employed to synthesize pillared bentonite, e.g., hydroxyaluminum, hydroxyzirconium, hydroxyiron, hydroxytitanium, and hydroxychromium [47-54]. Among these polycations, Al_{13} has the most popularity because of its keggin structure, high molecular weight, and high positive charge [55]. Pillared bentonite improves the removal efficiency of heavy metals [49, 56-63], Oxyanions [64-69], organic contaminants [64] and dyes [70-73]. So far, there are only two reports on the use of Al-pillared bentonite as adsorbent for the removal of Methylene Blue from aqueous solutions [74, 75].

The main objective of this work was to prepare hydroxy-aluminium pillared montmorillonite using Algerian bentonite. This new material was characterized by X-ray fluorescence spectrometry (XRF), X-ray

---

diffraction (XRD), Fourier transform infrared spectroscopy (FTIR) and nitrogen adsorption-desorption. The MB was chosen as adsorbate for its known strong adsorption onto materials. The adsorption of MB onto hydroxyl-aluminum pillared montmorillonite, including effects of contact time, solution pH, adsorbent dosage, initial MB concentration and temperature, was investigated by static adsorption experiments. We also studied the kinetics, isotherms and thermodynamics of adsorption.

Experimental

Materials and chemicals

The raw bentonite used in this study was obtained from deposits of Maghnia in western Algeria. It was purified by a method reported elsewhere [76]. The obtained fraction with a particle size < 2 μm were referred to as Na-Mt and employed in the pillaring process.

The dye MB and all chemicals (NaCl, Na_2CO_3, $AlCl_3.6H_2O$, NaOH, H_2SO_4) with the highest purity available, were obtained from Biochem Chemopharma company, France and used as received. All the solutions were prepared using distilled water. Chemical structure of the MB is shown in Scheme. 1.
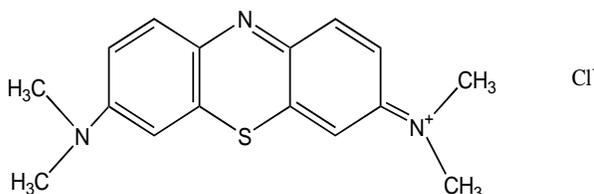
Scheme-1:   Molecular structure of MB.

Preparation of hydroxy-aluminum pillared montmorillonite

The first and main step in the preparation of hydroxyl-aluminum pillared montmorillonite was the preparation of the pillaring solution. The pillaring solution of hydroxyl-aluminum oligomeric cations ($[Al_{13}O_4(OH)_{24}(H_2O)_{12}]^{7+}$) was prepared following the procedure previously reported by Wang et al [77, 78]. It consists of addition drop by drop of Na_2CO_3 solution (0.4 mol/l) to $AlCl_3 \cdot 6H_2O$ solution (0.2 mol/l) under vigorous stirring at 80°C in order to obtain a OH^-/Al^{3+} molar ratio of 2.4. The resulting solution was stirred at 80°C for 2 h, and then aged for 24 h at room temperature. The second step in the preparation of hydroxyl-aluminum pillared montmorillonite was the intercalation by adding the pillaring solution to the water

suspension of Na-Mt (1wt %) at 80°C under vigorous stirring up to reach an Al_{13}^{7+}/Na-Mt ratio of 10 mmol/g. The mixture was stirred for an additional 2 h at 80°C and subsequently aging at 60°C for 24 h. The product was centrifuged, followed by washing with distilled water and the solid was dried at 80°C and ground into powder. This pillared sample was noted as OH-Al-Mt.

Characterization methods

The X-ray diffraction patterns were performed employing a Philips X'Pert MP diffractometer with Ni-filtered CuKα radiation using a powder sample. Chemical composition of the samples was determined by X-ray fluorescence spectrometry using a model Philips Magix Pro spectrometer with X-ray tube and Kα radiation for Rh. Spectrometer contains two flows: Ar + Methane and scintillation flow. Fourier transform infrared spectroscopy of the samples were measured using a "Spectrum Two" (Perkin Elmer, Inc.) spectrometer.

The spectra range for KBr is 8300 – 350 cm⁻¹ for the optic system and between 6000 and 550 cm⁻¹ for ZnSe mesures with a resolution of 2 cm⁻¹. Surface area and pore size distribution were determined by using N_2 as the sorbate at 77 K in a static volumetric apparatus (Micrometrics ASAP 2010 sorptometer). Samples (ca 0.2 g) were outgassed prior to use at 453 K for 16 h under vacuum (6.6 ∗ 10⁻⁹ bar). Surface areas were calculated employed the BET equation, while pore volumes were determined from N_2 uptake at a relative pressure (p/p_0) of N_2 equal to 0.99. The microporous surface and micropore volume were determined employing Horvath Kawazoe (HK) method [79]. Scanning electron microscopy (SEM) images of samples were obtained using a Quanta-650 scanning electron microscope (FEI).

Adsorption experiments

Batch experiments were carried out in water bath shaker (Heidoph Unimax 1010) using a glass flasks by adding 1 g/l of Na-Mt and OH-Al-Mt in 25 ml of initial concentration 100 mg/l of MB solutions and thermostated at 299 ± 1 K. The adsorption properties of these materials were studied as a function of contact time (10 - 420 min), solution pH (2 - 10), adsorbents dose (5 - 200 mg) and temperature (20, 30, and 50°C) for optimizing the operating conditions. Samples of 4 ml were withdrawn and centrifuged to separate the adsorbent from the solution. The supernatant was analyzed by UV–Vis spectrophotometer (Genesys-10) at the maximum wavelength of absorption λ_{max} = 665 nm. The MB concentration of each experiment was carried out with calibration curves obtained by plotting the optical densities as a function of MB concentration.

The pH of MB solutions was adjusted using 0.1 mol/l H_2SO_4 and 0.1 mol/l NaOH aqueous solutions, and was measured using a pH meter (AD 1030). Adsorption isotherm experiments were carried out by adding 1 g/l of adsorbents in 25 ml of MB solutions at different concentrations (4 - 150 mg/l) for desired contact time and pH. The amounts of adsorbed MB in the equilibrium per mass unit of the sample, q_e (mg/g), and the removal efficiency of the MB, E (%), were calculated according to Eqs. (1) and (2), respectively:

$$q_e = (C_0 - C_e) * \frac{V}{m} \qquad (1)$$

$$E\ (\%) = \frac{C_0 - C_e}{C_0} * 100 \qquad (2)$$

where C_0 is initial concentration of MB (mg/l), C_e is equilibrium concentration of MB (mg/l), V is the volume of MB solution (ml), and m is the mass of adsorbent (mg).

Results and Discussion

Characterization of the materials

The X-ray fluorescence data for the Na-Mt and OH-Al-Mt are reported in Table 1. As observed, the SiO_2 content in OH-Al-Mt was significantly lower than that in parent clay Na-Mt. This fact is principally due to the higher Al_2O_3 content which clearly indicates the insertion of Al_{13}^{7+} into the interlayer spacing as pillars, although it is possible that it can be also settled in minor amounts over the montmorillonite sheets. Table 1 also illustrates that the amount of Na_2O in the OH-Al-Mt was significantly decreased after pillaring processes. This result is in agreement with previous finding [55, 80-81], denoting that this decrease is mainly due to the cation exchange between Na^+ and Al_{13}^{7+}.

X-ray diffraction patterns and relative basal spacing of Na-Mt and OH-Al-Mt are illustrated in Fig. 1 and Table 1. The angle reflections due to the basal d_{001} reflection of silicate layers allowed us to obtain information about the effect of intercalation on the basal spacing of the clay. In particular, it can clearly be seen that the diffraction peak at $2\theta = 7.04°$ of Na-Mt is shifted to lower angle around 4.78° in OH-Al-Mt. This shift clearly indicates an enlargement of the basal spacing of the clay as a consequence of the pillaring process (from 12.5 Å of the parent clay to about 18.5 Å of the OH-Al-Mt, see in Table 1). This value confirms values previously reported for the used Al_{13} as a pillaring species [73, 82, 83]. The observed enlargement of the basal spacing is due to the intercalation of Al_{13}^{7+} cations between montmorillonite layers. Fig. 1 also shows that the (001) peak of OH-Al-Mt was lower

intensity than that of the starting Na-Mt in agreement with previous results obtained by Tepmatee and Siriphannon [80].
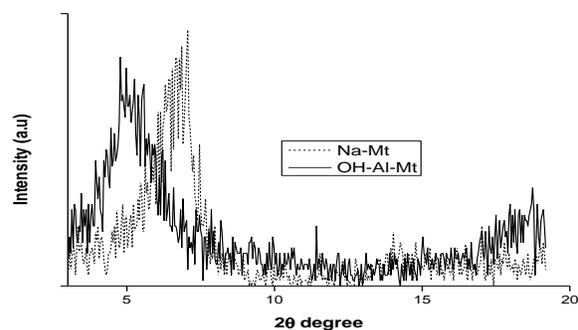
Fig. 1:   XRD patterns of Na-Mt and OH-Al-Mt.

The textural properties of the samples are shown in Table 1. It is clear that the BET surface area and pore volume of OH-Al-Mt were greater than those of Na-Mt, which are in agreement with results previously reported [55, 73, 75, 77, 78]. Micropores are known to contribute to most of the adsorption capacity [84, 85]. After modification with Al_{13}, the micropore surface area and micropore volume increased to 127.3 m^2/g and 0.07 cm^3/g, respectively. These results could be assigned to the insertion of Keggin-Al_{13} into the interlayers of the montmorillonite.

The nitrogen adsorption desorption isotherms for the samples are presented in Fig. 2a. The isotherms shapes are composite type I and type IV isotherms. Similar shapes have been reported for other pillared materials [86, 87]. At low relative pressures ($P/P_0 < 0.5$), isotherms were characterized by type I isotherms according to the Brunauer, Deming, Deming and Teller classification (BDDT) [88], which is characteristic of microporous systems [89]. Note that, a significant higher amount of adsorbed nitrogen molecules were achieved for OH-Al-Mt compared to the Na-Mt, indicating the opening of the pore structure of the clay after the pillaring process and so, the improvement of its adsorption capacity. On the other hand, the plot of samples isotherms at higher P/P_0 values would correspond to the type IV, which is characteristic of materials having relatively large pores. Moreover, the presence of a hysteresis loop in the isotherms (type H_3 according the International Union of Pure and Applied Chemistry (IUPAC) classification [89], indicates some degree of mesoporosity (mesoporosity arises from stacking defects inherent in the clay itself, as evidenced by the hysteresis loop seen in the adsorption isotherm of the starting clay). The hysteresis loop, characteristic of materials with slit-like pores, is consistent with the structure expected for materials prepared by expanding a laminar structure.

Table-1: Chemical composition (wt%), basal spacing (d_{001}) and textural properties of Na-Mt and OH-Al-Mt.

Adsorbent	Chemical composition (Wt%)			Basal spacing	Textural properties			
	Al_2O_3	SiO_2	Na_2O	d_{001} (Å)	BET surface area (m²/g)	Micropore Surface area (m²/g)	Micropore volume (cm³/g)	Pore volume (cm³/g)
Na-Mt	17.75	58.52	2.72	12.5	59.3	13.0	0.009	0.11
OH-Al-Mt	25.26	49.68	0.17	18.5	182.9	127.3	0.069	0.18
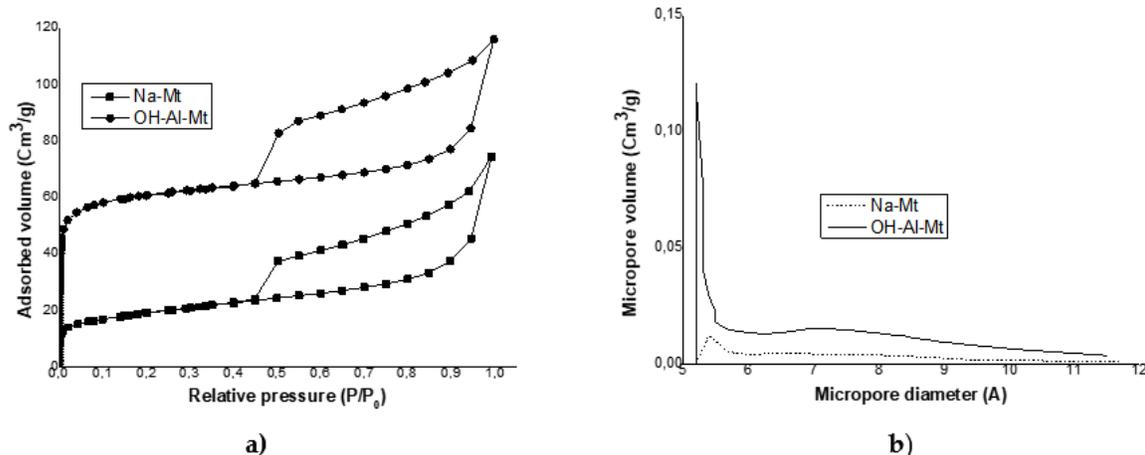
Fig. 2:   Nitrogen adsorption-desorption results: a) isotherms and b) micropore size distribution (HK method).

The micropore size distribution curves (Fig. 2b) were calculated from Horvath-Kawazoe (H-K) method. The primary peaks at about 5.2 - 5.4 Å in the curves of samples correspond to the main population of pores, but with a continuous distribution of pores in the range of 5.4 - 11 Å, which are in agreement with results previously reported [78].

The FTIR spectra of Na-Mt and OH-Al-Mt in the range of 4000–400 cm^{-1} are shown in Fig. 3. The band at about 3617 cm^{-1} is assigned to the stretching vibration of octahedral OH groups, which are attached to Al^{3+} or Mg^{2+} [90]. The absorption peak at 1634 cm^{-1} is attributed to OH deformation of interlayer water. The intensity of this band changed, which could be explained due to some changes of the H_2O content with the replacement of the intercalated Al polycations [91]. The most intense band at 990 cm^{-1} shifted to 1003 cm^{-1} near the Si-O stretching vibration in the tetrahedral sheet, the intensity also decreased from Na-Mt to OH-Al-Mt. This finding is in agreement with other investigations obtained by Zhao et al [55] that demonstrated that Al_{13} species were intercalated into the interlayers of the montmorillonite. The band situated at 515 and 463 cm^{-1} characterize the montmorillonite and correspond to the Si-O bending vibrations.

SEM was used to study the changes in morphology of Na-Mt and OH-Al-Mt (Fig. 4). It can be seen that the Na-Mt is constituted of fine particles and the morphologies of these particles indicated that the sample had the lamellar structure (Fig. 4a). After modification with Al_{13}, the OH-Al-Mt is composed of fine and large particles, explaining that some of lamellas were disposed to form a stacking structure (Fig. 4b), which was consistent with extended the interlayer space, increased the surface area and consequently increased adsorption capacity.
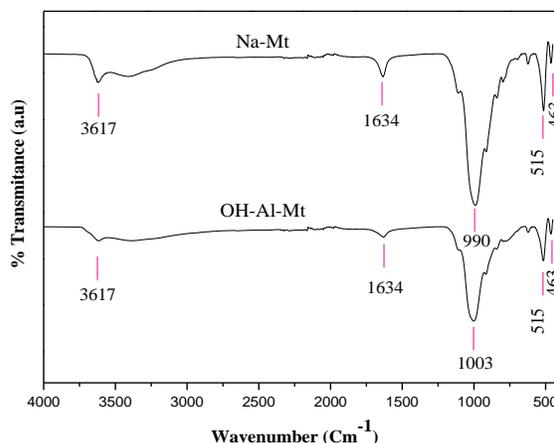
Fig. 3:   FTIR spectra of Na-Mt and OH-Al-Mt.

(a)   **(b)**
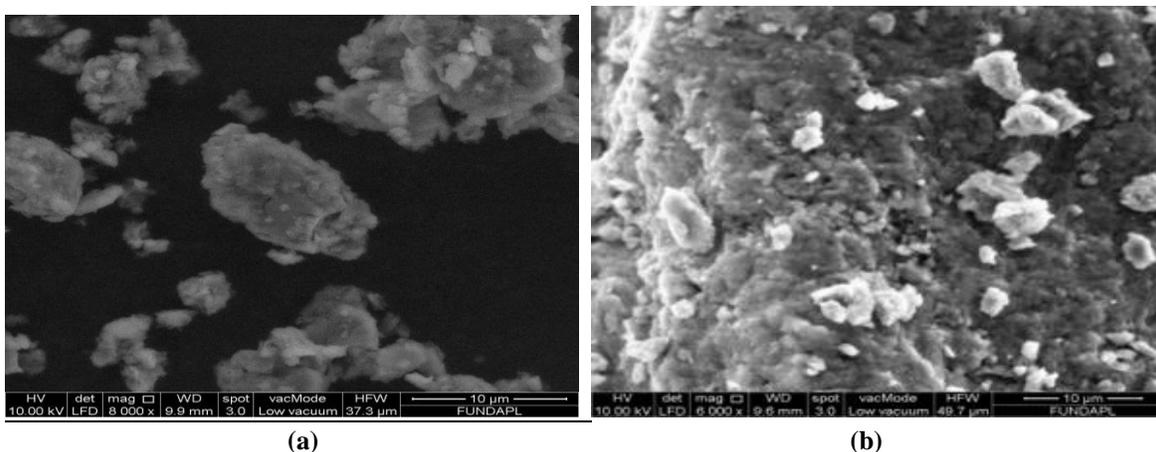
Fig. 4:   SEM images of Na-Mt (a) and OH-Al-Mt (b)
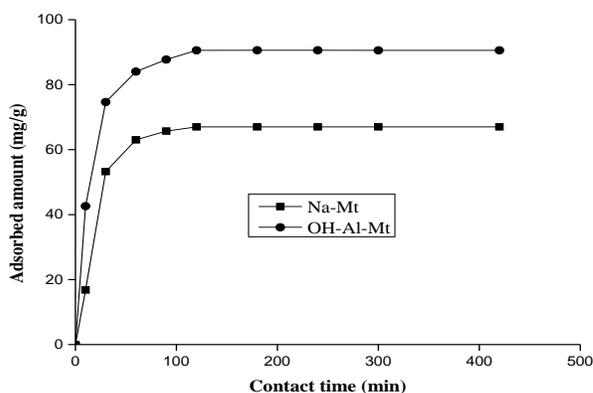
Fig. 5: Effect of contact time on the adsorption of MB (MB: 100 mg/l, adsorbent dose: 1 g/ l).

Adsorption experiments

Effect of contact time and adsorption kinetics

Several studies were established the effect of contact time on the amounts of adsorbed dye onto a fixed adsorbent mass [92-95]. The effect of contact time on the adsorption capacities of Na-Mt and OH-Al-Mt for MB was illustrated in Fig. 5. As observed, the rate of adsorption was fast at initial 30 min due to the adsorption of MB on the external surface of adsorbents. After that, slow adsorption occurred that referred to the MB diffused into the pores and was absorbed by the internal surface of the adsorbents. The last stage reflects the adsorption equilibrium of adsorbents within 120 min and the final adsorption capacities were calculated to be about 67 mg/g and 90 mg/g for Na-Mt and OH-Al-Mt, respectively. Subsequently, no further adsorption was observed. Hence, the optimum contact time was chosen as 120 min. However, the pillared clay has a higher adsorption capacity than the Na-Mt. It can be related to the pillaring process which results in materials with altered chemical composition, extended the interlayer space, increased the surface area and consequently increased adsorption capacity. Additionally, Al_{13} had a higher positive charge (+7) than Na (+1), leading to the enhancement of adsorption performance of the modified montmorillonite [55].

The adsorption kinetics is an essential feature on the investigation of the pollutants decolorization. In order to investigate the adsorption kinetics and mechanism of MB adsorption on adsorbents, pseudo-first order and pseudo-second order models were used to fit the kinetics process. The pseudo-first-order equation in linear form [96] is given by:

$$\log(q_e - q_t) = \log q_e - \left(\frac{k_1}{2.303}\right)t \qquad (3)$$

and the expression of the linear form of the pseudo-second-order model [97, 98] is given as:

$$\frac{t}{q_t} = \left(\frac{1}{k_2 q_e^2}\right) + \left(\frac{1}{q_e}\right)t \qquad (4)$$

where q_e and q_t are the amounts of MB (mg/g) adsorbed on the adsorbent at equilibrium and at a given time t (min), respectively. k_1 (min^{-1}) and k_2 (g/mg.min) are the pseudo-first-order and the pseudo-second-order rate constants, respectively.

Table 2 illustrates the kinetic parameters and correlation coefficients values. It was found that of the both adsorbents, the pseudo-second-order model fitted well the experimental results with $R^2 = 0.99$. Similar reports are available in literature [4-6, 18, 29, 35, 73, 99-108].

Table-2: Adsorption kinetics parameters of MB on Na-Mt and OH-Al-Mt.

Adsorbent	Pseudo-first order model			Pseudo-second order model		
	q_e (mg/g)	K_1 (min^{-1})	R^2	q_e (mg/g)	K_2 (g/mg. min)	R^2
Na-Mt	64.71	0.044	0.986	71.42	$1.16*10^{-3}$	0.996
OH-Al-Mt	55.46	0.032	0.976	100	$1.44*10^{-3}$	0.999
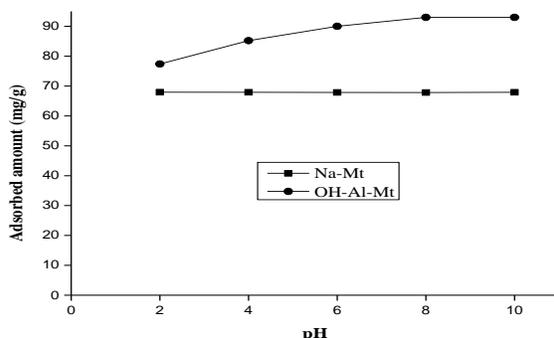
Fig. 6: Effect of solution pH on the adsorption of MB (MB: 100 mg/l, adsorbent dose: 1 g/l, contact time: 120 min).

Effect of solution pH

The pH changing of the aqueous solution plays an important role in the adsorption process [93]. The effects of solution pH on adsorbents were examined over the pH range of 2-10 (Fig. 6). It is clear that the adsorption of MB by Na-Mt was not remarkably affected by pH. Similar results have been reported for the sorption of cationic dye by montmorillonite and palygorskite [109-111]. For OH-Al-Mt, the data indicate the removal of MB dye increased with increasing pH solution up to pH 8. However, the MB uptake capacities were not changed from pH 8 to 10. Point of zero charge (pHpzc) is an important factor which indicates the adsorbent surface charge [112]. Adsorbents have a negative charge on their surface when pH $_{solution}$ > pH$_{PZC}$, while they have a positive charge when pH $_{solution}$ < pH$_{PZC}$ [74]. The pHpzc of the OH-Al-Mt was found to be 4.5. Since MB existed as cations (Scheme 1), at pH < 4.5, the surface of the OH-Al-Mt becomes positively charged, resulting in electrostatic repulsion due to the same positively charged MB molecules. Also, there was competition between protons and MB ions for the available adsorption sites. In contrast, at pH > 4.5, the negatively charged surface of adsorbent favors uptake of cationic dye MB due to increased electrostatic attraction. Furthermore, there was a certain adsorption capacity of MB for the entire pH region and can be due to (i) hydrogen bonding between –N of MB and surface –OH groups or hydroxide groups of aluminum polycations proceeding in interlayer space, (ii) interactions among π electronic clouds of MB and cations such as

Na$^+$, Al$_{13}$$^{+7}$ present on the surface of the clays and (iii) hydrophobic character which favors the adsorption of MB with respect to water. Similar results were obtained by previously reports [4, 33, 99, 113-115]. The pH of wastewater is 6-9 and the natural pH of the MB solution is 6.1. Also, we have slightly difference between the MB removal at pH = 6 and pH = 8 (90 % at pH = 6 and 93% at pH = 8). Therefore, we retained the pH solution without adjustment in the rest of adsorption experiments

Effect of adsorbent dose

In order to determine a minimum adsorbent amount that is economically realizable in wastewater treatment process, we have investigated the efficiency of sorbent dosages on the elimination of MB. Fig. 7 showed that the % removal of MB increased from 53% to 67% and 78% to 90% for Na-Mt and OH-Al-Mt, respectively, as adsorbent amount increased from 0.2 to 1 g/l. This fact can be assigned to increase in the adsorptive surface area and adsorption sites that can take up MB cations become more available. Subsequently, the removal rate did not affected by further increase in adsorbent dose, indicating saturation state. When the adsorbent dosage is low, the dye ions can easily access the adsorption sites by contrast when the adsorbent dosage is high, the dye ions can hardly access the adsorption sites until the attainment of equilibrium [116]. The percentage removal for Na-Mt was lower than that for modified clay, indicated that the adsorption ability of OH-Al-Mt was dramatically enhanced by Al$_{13}$ modification. According to this experiment, 1 g/l adsorbent dose (optimal adsorbent dosage) was chosen for the successive experiments.

Fig. 7: Effect of adsorbent dose on MB removal (MB: 100 mg/l, contact time: 120 min).

Adsorption isotherms

The adsorption isotherms were carried out at different initial concentrations (4 to 200 mg/l) during 120 minutes at room temperature and adsorbent dose 1g/l. The isotherms are formed by plot adsorbed amount of MB versus equilibrium concentration. The Fig. 8 depicts the adsorption of MB by Na-Mt and OH-Al-Mt. It can be seen that for both adsorbents, the amount of Methylene Blue adsorbed increases with an increase in initial adsorbate concentration, due to the increased driving force of the concentration gradient [120]. A similar effect has been observed with previously reported [18, 105]. The OH-Al-Mt exhibited higher adsorption capacity than the Na-Mt in same operating conditions, due to the altered chemical composition, enlarged the interlayer space and their higher BET specific surface area.

Fig. 8: Adsorption isotherms of MB onto Na-Mt and OH-Al-Mt (contact time: 120 min, adsorbent dose: 1 g/l).

In order to comprehend the interactions between MB and the adsorbent, adsorption isotherm models, including the Langmuir [118], Freundlich [119] and Temkin [120] models were tested. The linear forms of the Langmuir, Freundlich and Temkin models can be expressed using Eqs. (5), (6) and (7), respectively:

$$\frac{C_e}{q_e} = \frac{1}{K_L \cdot q_m} + \left(\frac{1}{q_m}\right) C_e \qquad (5)$$

$$\log q_e = \log K_F + \left(\frac{1}{n}\right) \log C_e \qquad (6)$$

$$q_e = B_T \ln K_T + B_T \ln C_e \qquad (7)$$

where q_m (mg/g) and K_L (l/mg) are Langmuir constants respectively related to the maximum adsorption capacity and the adsorption energy. K_F and n are Freundlich constants respectively related to the adsorption capacity $((mg/g)(l/mg)^n)$ and the adsorption intensity. $B_T = RT/b$, T is the temperature (K), R is the universal gas constant (8.314 J/mol K), and b is the Temkin constant related to heat of adsorption (J/mol).

The fitted constants for Langmuir, Freundlich and Temkin isotherm models at room temperature are summarized in Table-3. The coefficient of determination (R^2) values in the Freundlich isotherm model were above 0.99, which were higher than that for the Langmuir and Temkin isotherms, indicating a very good mathematical fit by this model. Similar results have been reported for the adsorption of Basic Fuchsin, Basic Green and Acid Turquoise Blue A [73] by hydroxy-aluminum pillared bentonite, direct orange 34 [121] by halloysitic clay, methylene blue [113] by zeolite–activated carbon composite. Generally, the value of n in the range of 2–10 indicates good, 1–2 moderately difficult and below 1 poor adsorption characteristics [44]. The measured 1/n was below to the unit, which means the adsorption was favorable. In addition to that, adsorption of any contaminant is considered favorable $(0 < K_L < 1)$; unfavorable $(K_L > 1)$, linear $(K_L = 1)$ and irreversible $(K_L = 0)$ [44]. The measured K_L were below to the unit, indicated the favorable adsorption of MB onto both adsorbents.

For comparison, results obtained from the literature on Methylene Blue monolayer adsorption by various clays are summarized in Table 4. It is seen that the OH-Al-Mt shows a high affinity for MB molecules and the q_m of the Langmuir adsorption isotherm is much higher to that in previous results [74, 75, 103, 106, 114, 122-131].

Effects of temperature and thermodynamic studies

Temperature is an important parameter for the adsorption process. A plot of the MB uptake as a function of temperature (293, 313 and 333 K) is shown in Fig. 9. The adsorbed amounts of MB were decreased from 67.36 to 64.9 mg/g and 90.58 to 87.36 mg/g for Na-Mt and OH-Al-Mt, respectively, as temperature increased from 293 K to 333 K. This result shows that adsorption onto the adsorbents is favorable at low temperature and thus suggesting that the adsorption process is exothermic. According to [104], the dye molecules escape from the solid phase to the solution with increase the temperature.

Table-3: Isotherm model parameters for adsorption of MB onto Na-Mt and OH-Al-Mt.

Sample	Langmuir				Freundlich			Temkin		
	q_m (mg/g)	K_L (l/mg)	R^2	1/n	K_F (mg/g)	R^2	B_T	K_T (l/mg)	R^2
Na-Mt	111.11	0.024	0.95	0.89	2.96	0.998	22.4	0.56	0.87
OH-Al-Mt	142.86	0.30	0.91	0.44	28.97	0.99	14.69	29.75	0.80

Table-4: Comparison of monolayer adsorption of MB onto various clays.

Adsorbent	Adsorption capacity (mg/g)	Reference
Kaolin	52.76	[122]
Kaolinite	77	[123]
Sepiolite	57.38	[124]
Sepiolite	110	[125]
Clay	6.3	[126]
Raw ball clay	34.65	[114]
Modified Ball clay	100	[114]
Spent activated clay	127.50	[127]
Zn-PILC	27	[74]
Montmorillonite	110	[128]
Tsu-Mont	73	[75]
Chitosan/bentonite	95.24	[129]
Carbon/montmorillonite composites	82.6	[130]
Montmorillonite modified with iron oxide	69.11	[106]
Fe_3O_4/Mt	106.38	[103]
Mt/$CoFe_2O_4$ composite	97.75	[131]
Al-PILC	21	[74]
Alumina-pillared clays	40	[75]
Na-Mt	111.11	[This work]
OH-Al-Mt	142.85	[This work]

Fig. 9: Effects of temperature on the MB adsorption capacity of Na-Mt and OH-Al-Mt.

The thermodynamic behavior of the adsorption of MB onto the adsorbents were defined by Gibb's free enthalpy (ΔG˚: kJ/mol), enthalpy (ΔH˚: kJ/mol) and entropy (ΔS˚: J/mol.K) and were calculated using the following equations [104]

$$\ln\left(\frac{q_e m}{C_e}\right) = \left(\frac{\Delta S°}{R}\right) - \left(\frac{(\Delta H)°}{RT}\right) \qquad (8)$$

$$\Delta G° = \Delta H° - T * \Delta S° \qquad (9)$$
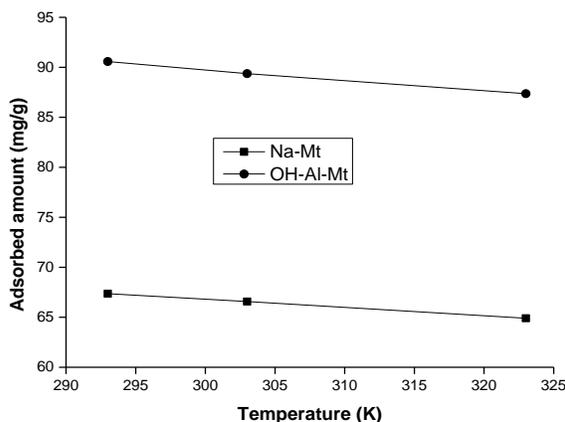
where m is the adsorbent dose (1 g/l), C_e is the equilibrium concentration (mg/l) of the MB in solution, q_e is the amount of MB adsorbed at equilibrium (mg/g), R is the gas constant (8.314 J/mol K) and T is the temperature (K).

The values of ΔH˚ and ΔS˚ are calculated from the slope (($-\dfrac{\Delta H°}{R}$) and the intercept ($\dfrac{\Delta S°}{R}$) of the plots of ln (q_e/C_e) against 1/T (figure not shown). The ΔG˚ values were calculated using Eq. (9). The determined values of the thermodynamic parameters are given in Table 5. The values of ΔG° were found to be negative under various temperatures which indicated the favorable nature of MB adsorption onto adsorbents and spontaneous process under the experiment condition. The negative value of ΔH° suggests that the adsorption of MB onto adsorbents was exothermic and the negative ΔS° value can be attributed to the decline in the disorder at the solid/solution interface. Generally, when the ΔH° < 25 kJ/mol, the adsorption is physical and when ΔH° is in the range 40–200 kJ/mol, the adsorption is chemical [99]. In this study, ΔH° is less than 25 kJ/mol and thus adsorption is physical.

Table-5: Thermodynamics parameters of MB adsorption onto the Na-Mt and OH-Al-Mt.

Adsorption system	ΔH˚ (kJ/mol)	ΔS˚ (J/mol.K)	ΔG˚ (kJ/mol)		
			293 K	303 K	323 K
Na-Mt	-2.96	-4.07	-1.77	-1.74	-1.65
OH-Al-Mt	-8.76	-11.14	-5.50	-5.39	-5.16

Conclusions

In this work, the removal of MB from water solutions was investigated by employing as adsorbents a purified raw montmorillonite (Na-Mt) and hydroxy-aluminum pillared montmorillonite (OH-Al-Mt). OH-Al-Mt had a good ordered layers structure with insertion of Al_{13}^{7+} cations, which caused an increase in the clay spacing. Its specific surface area is about three times larger than that of the parent Na-Mt due principally to the creation of a remarkable microporous network.

The optimized conditions for MB dye removal by adsorbents were confirmed at 1 g/l adsorbent dosage, equilibrium time 120 min, natural pH (6.1) and decreased with the increase of

temperature. The adsorption of Methylene Blue onto both clays obeyed pseudo-second-order kinetics. The pillared clay has a higher adsorption capacity than the Na-Mt. The best equilibrium adsorption isotherm fit was obtained with the Freundlich model. Thermodynamic studies showed that the adsorption is spontaneous and exothermic process.

Acknowledgments

References

1. T. Robinson, G. McMullan, R. Marchant and P. Nigam, Remediation of dyes in textile effluent: a critical review on current treatment technologies with a proposed alternative, *Bioresour. Technol.*, **77**, 247 (2001).

2. S. Rasalingam, R. Peng and R.T. Koodali, An insight into the adsorption and photocatalytic degradation of rhodamine B in periodic mesoporous materials, *Appl. Catal. B: Environ.*, **174**, 49 (2015).

3. Y. Gao, Y. Guo and H. Zhang, Iron modified bentonite: Enhanced adsorption performance for organic pollutant and its regeneration by heterogeneous visible light photo-Fenton process at circumneutral pH, *J. Hazard. Mater.*, **302**, 105 (2016).

4. D. Pathania, S. Sharma and P. Singh, Removal of methylene blue by adsorption onto activated carbon developed from Ficus carica bast, *Arab. J. Chem.*, **10**, S1445 (2017).

5. F. Liu , H. Zou, J. Hu, H. Liu, J. Peng, Y. Chen, F. Lua and Y. Huo, Fast removal of methylene blue from aqueous solution using porous soy protein isolate based composite beads, *Chem. Eng. J.*, **287**, 410 (2016).

6. S. Kittappa, S. Pichiah, J.R. Kim, Y. Yoon, S.A. Snyder and M. Jang, Magnetised nanocomposite mesoporous silica and its application for effective removal of methylene blue from aqueous solution, *Sep. Pur. Technol.*, **153**, 67 (2015).

7. Y.Y. Lau, Y.S. Wong, T.T. Teng, N. Morad, M. Rafatullah and S.A. Ong, Coagulation flocculation of azo dye Acid Orange 7 with green refined laterite soil, *Chem. Eng. J.*, **246**, 383 (2014).

8. B. Kokabian, B. Bonakdarpour and S. Fazel, The effect of salt on the performance and characteristics of a combined anaerobic–aerobic biological process for the treatment of synthetic wastewaters containing Reactive Black 5, *Chem. Eng. J.*, **221**, 363 (2013).

9. V.A. Sakkas, M.A. Islam, C. Stalikas and T.A. Albanis, Photocatalytic degradation using design of experiments: a review and example of the Congo red degradation, *J. Hazard. Mater.*, **175**, 33 (2010).

10. M.E. Fernandez, G.V. Nunell, P.R. Bonelli and A.L. Cukierman, Activated carbon developed from orange peels: batch and dynamic competitive adsorption of basic dyes, *Ind Crops Prod.*, **62**, 437 (2014).

11. N.K. Rotte, S. Yerramala, J. Boniface and V.V.S.S. Srikanth, Equilibrium and kinetics of Safranin O dye adsorption on MgO decked multi-layered graphene, *Chem. Eng. J.*, **258**, 412 (2014).

12. P. Luo, Y. Zhao, B. Zhang, J. Liu, Y. Yang and J. Liu, Study on the adsorption of Neutral Red from aqueous solution onto halloysite nanotubes, *Water Res.*, **44**, 1489 (2010).

13. Y. Bulut and H. Aydın, A kinetics and thermodynamics study of methylene blue adsorption on wheat shells, *Desalination.*, **194**, 259 (2006).

14. C.X. Gui, Q.Q. Wang, S.M. Hao, J. Qu, P.P. Huang, C.Y. Cao, W.G. Song and Z.Z. Yu, Sandwich like magnesium silicate/reduced graphene oxide nanocomposite for enhanced Pb^{2+} and methylene blue adsorption, *ACS Appl. Mater. Interfaces.*, **6**, 14653 (2014).

15. H. Yan, X. Tao, Z. Yang, K. Li, H. Yang, A.M. Li and R.S. Cheng, Effects of the oxidation degree of graphene oxide on the adsorption of methylene blue, *J. Hazard. Mater.*, **268**, 191 (2014).

16. S.T. Yang, S. Chen, Y.L. Chang, A.N. Cao, Y.F. Liu and H.F. Wang, Removal of methylene blue from aqueous solution by graphene oxide, *J. Colloid Interface Sci.*, **359**, 24 (2011).

17. Z. Wu, L. Zhang, Q. Guan, P. Ning and D. Ye, Preparation of a-zirconium phosphate-pillared reduced graphene oxide with increased adsorption towards methylene blue, *Chem. Eng. J.*, **258**, 77 (2014).

18. L. Chen, Y. Lia,, Q. Du, Z. Wang, Y. Xia, E. Yedinak, J. Lou and L. Ci, High performance agar/graphene oxide composite aerogel formethylene blue removal, *Carbohydr Polym.*, **155**, 345 (2017).

19. L. Xiong, Y. Yang, J.X. Mai, W.L. Sun, C.Y. Zhang, D.P. Wei, Q. Chen and J.R. Ni, Adsorption behavior of methylene blue onto titanate nanotubes, *Chem. Eng. J.*, **156**, 313 (2010).

20. H. Mittal, A. Maity and S.S. Ray, Synthesis of co-polymer-grafted gum karaya and silica hybrid organic–inorganic hydrogel nanocomposite for the highly effective removal of methylene blue, *Chem. Eng. J.*, **279**, 166 (2015).

21. L.Z. Bai, Z.P. Li, Y. Zhang, T. Wang, R.H. Lu, W.F. Zhou, H.X. Gao and S.B. Zhang, Synthesis of water-dispersible graphene-modified magnetic polypyrrole nanocomposite and its ability to efficiently adsorb methylene blue from aqueous solution, *Chem. Eng. J.*, **279**, 757 (2015).

22. M.N. Chong, Z.Y. Tneu, P.E. Poh , B. Jin and R. Aryal, Synthesis, characterisation and application of TiO$_2$ –zeolite nanocomposites for the advanced treatment of industrial dye wastewater. *J Taiwan Inst Chem E.*, **50**, 288 (2015).

23. M.A. Salam, Synthesis and characterization of novel manganese oxide nanocorals and their application for the removal of methylene blue from aqueous solution, *Chem. Eng. J.*, **270**, 50 (2015).

24. Y.J. Xie, B. Yan, H.L. Xu, J. Chen, Q.X. Liu, Y.H. Deng and H.B. Zeng, Highly regenerable Mussel-inspired Fe$_3$O$_4$@polydopamine-Ag core-shell microspheres as catalyst and adsorbent for methylene blue removal, *ACS Appl. Mater. Interfaces.*, **6**, 8845 (2014).

25. L.D.L. Miranda, C.R. Bellato, M.P.F. Fontes, M.F. de Almeida, J.L. Milagres and L.A. Minim, Preparation and evaluation of hydrotalcite-iron oxide magnetic organocomposite intercalated with surfactants for cationic methylene blue dye removal, *Chem. Eng. J.*, **254**, 88 (2014).

26. J.Z. Guo, B. Li, L. Liu and K. Lv, Removal of methylene blue from aqueous solutions by chemically modified bamboo, *Chemosphere.*, **111**, 225 (2014).

27. L. Zhou, J.C. Huang, B.Z. He, F. Zhang and H.B. Li, Peach gum for efficient removal of methylene blue and methyl violet dyes from aqueous solution, *Carbohydr. Polym.*, **101**, 574 (2014).

28. X.Y. Huang, H.T. Bu, G.B. Jiang and M.H. Zeng, Cross-linked succinyl chitosan as an adsorbent for the removal of methylene blue from aqueous solution, *Int. J. Biol. Macromol.*, **49**, 643 (2011).

29. A.B. Albadarin, M.N. Collins, M. Naushad, S. Shirazian, G. Walker and C. Mangwandi, Activated lignin-chitosan extruded blends for efficient adsorption of methylene blue, *Chem. Eng. J.*, **307**, 264 (2017).

30. L.H. Ai, M. Li and L. Li, Adsorption of methylene blue from aqueous solution with activated carbon/cobalt ferrite/alginate composite beads: kinetics, isotherms, and thermodynamics, *J. Chem. Eng. Data.*, **56**, 3475 (2011).

31. J.A. Yang and K.Q. Qiu, Preparation of activated carbons from walnut shells via vacuum chemical activation and their application for methylene blue removal, *Chem. Eng. J.*, **165**, 209 (2010).

32. K. Mahapatra, D.S. Ramteke and L.J. Paliwal, Production of activated carbon from sludge of food processing industry under controlled pyrolysis and its application for methylene blue removal, *J. Anal. Appl. Pyrolysis.*, **95**, 79 (2012).

33. A.F. Hassan and H. Elhadidy, Production of activated carbons from waste carpets and its application in methylene blue adsorption: Kinetic and thermodynamic studies, *J. Environ. Chem. Eng.*, **5**, 955 (2017).

34. S.L. Lin, Z.L. Song, G.B. Che, A. Ren, P. Li and C.B. Liu, J.S. Zhang, Adsorption behavior of metal-organic frameworks for methylene blue from aqueous solution. *Microporous and Mesoporous Mater.*, **193**, 27 (2014).

35. Ö. Şahin and M. Kaya, C. Saka, Plasma-surface modification on bentonite clay to improve the performance of adsorption of methylene blue, *Appl Clay Sci.*, **116–117**, 46 (2015).

36. T. Shichi and K. Takaqi, Clay minerals as photochemical reaction fields. J. Photochem. *Photobiol. C. Photochem. Rev.*, **1**, 113 (2000).

37. Q. Hu, S. Qiao, F. Haghseresht, M. Wilson and G. Lu, Adsorption study for removal of basic red dye using bentonite, *Ind. Eng. Chem. Res.*, **45**, 733 (2006).

38. S.S. Tahir and N. Rauf, Removal of a cationic dye from aqueous solutions by adsorption onto bentonite clay, *Chemosphere.*, **63**, 1842 (2006)..

39. E. Bulut, M. Özacar and İ. Ayhan Sengil, Equilibrium and kinetic data and process design for adsorption of congo red onto bentonite, *J. Hazard. Mater.*, **154**, 613 (2008).

40. E. Eren and B. Afsin, Investigation of a basic dye adsorption from aqueous solution onto raw and pre-treated bentonite surfaces, *Dyes Pigm.*, **76**, 220 (2008).

41. J. Wei, R. Zhu, J. Zhu, F. Ge, P. Yuan, H. He and C. Ming, Simultaneous sorption of crystal violet and 2-naphthol to bentonite with different CECs, *J. Hazard. Mater.*, **166**, 195 (2009).

42. S. Hong, C. Wen, J. He, F. Gan and Y.S. Ho, Adsorption thermodynamics of methylene blue

onto bentonite, *J. Hazard. Mater.*, **167**, 630 (2009).

43. H. Tahir, U. Hammed, M. Sultan and Q. Jahanzeb, Batch adsorption technique for the removal of malachite green and fast green dyes by using montmorillonite clay as adsorbent. *Afr. J. Biotechnol.*, **9**, 8206 (2010).

44. M.T. Amin, A.A. Alazba and M. Shafiq, Adsorptive Removal of Reactive Black 5 from Wastewater Using Bentonite Clay: Isotherms, Kinetics and Thermodynamics, *Sustainability.,* **7**, 15302 (2015).

45. C. Yang, Y. Zhu, J. Wang, Z. Li, X. Su and C. Niu, Hydrothermal synthesis of TiO_2–WO_3– bentonite composites: Conventional versus ultrasonic pretreatments and their adsorption of methylene blue, *Appl Clay Sci.*, **105–106**, 243 (2015).

46. R.L. Zhu, L.Z. Zhu, J.X. Zhu, F. Ge and T. Wang, Sorption of naphthalene and phosphate to the CTMAB–Al_{13} intercalated bentonites. *J. Hazard. Mater.*, **168**, 1590 (2009).

47. L. Gu, J.L. Xu, L. Lv, B. Liu, H.N. Zhang, X. Yuand Z.N. Luo, Dissolved organic nitrogen (DON) adsorption by using Al-pillared bentonite, *Desalination.*, **269**, 206 (2011).

48. B.G. Mishra and G.R. Rao, Physicochemical and catalytic properties of Zr-pillared montmorillonite with varying pillar density, *Microporous and Mesoporous Mater.*, **70**, 43 (2004).

49. W. Matthes, F.T. Madsen and G. Kahr, Sorption of heavy-metal cations by Al and Zr hydroxy-intercalated and pillared bentonite. *Clays Clay Miner.*, **47**, 617 (1999).

50. W. Matthes and G. Kahr, Sorption of organic compounds by Al- and Zr-hydroxy intercalated and pillared bentonite. *Clays Clay Miner.*, **48**, 593 (2000).

51. O. Bouras, J.C. Bollinger, M. Baudu, Effect of humic acids on pentachlorophenol sorption to cetyltrimethylammonium-modified, Fe- and Al-pillared montmorillonites, *Appl. Clay Sci.*, **50**, 58 (2010).

52. P. Yuan, F. Bergaya, Q. Tao, M. Fan, Z. Liu, J. Zhu and H. He, A combined study by XRD, FTIR, TG and HRTEM on the structure of delaminated Fe-intercalated/pillared clay. *J. Colloid Interface Sci.*, **324**, 142 (2008).

53. P. Na, X. Jia, B. Yuan, Y. Li, J. Na, Y. Chen and L. Wang, Arsenic adsorption on Ti-pillared montmorillonite. *J. Chem. Technol. Biotechnol.*, **85**, 708 (2010).

54. F. Tomul and S. Balci, Characterization of Al, Cr-pillared clays and CO oxidation, *Appl. Clay Sci.*, **43**, 13 (2009).

55. S. Zhao, C. Feng, X. Huang, B. Li , J. Niu and Z. Shen, Role of uniform pore structure and high positive charges in the arsenate adsorption performance of Al_{13}-modified montmorillonite, *J. Hazard. Mater.*, **203– 204**, 317 (2012).

56. Y.L. Zhang, Y.M. Li, J.F. Li, G.D. Sheng, Y. Zhang and X.M. Zheng, Enhanced Cr(VI) removal by using the mixture of pillared bentonite and zero-valent iron, *Chem. Cent. J.*, **185–186**, 243 (2012).

57. J.B. Harsh and H.E. Doner, Specific sorption of copper on a hydroxyl–aluminum– montmorillonite complex, *Soil Sci. Soc. Am. J.*, **48**, 1034 (1984).

58. B. Lothenbach, G. Furrer and R. Schulin, Immobilization of heavy metals by polynuclear aluminium and montmorillonite compounds, *Environ. Sci. Technol.*, **31**, 1452 (1997).

59. B. Lothenbach, R. Krebs, G. Furrer, S.K. Gupta and R. Schulin, Immobilization of cadmium and zinc in soil by Al-montmorillonite and gravel sludge, *Eur. J. Soil Sci.*, **49**, 141 (1998).

60. B. Lothenbach, G. Furrer, H. Schärli and R. Schulin, Immobilization of zinc and cadmium by montmorillonite compounds: effects of aging and subsequent acidification, *Environ. Sci. Technol.*, **33**, 2945 (1999).

61. L. Bergaoui, I. Mrad, J.F. Lambert and A. Ghorbel, A comparative study of the acidity toward the aqueous phase and adsorptive properties of Al_{13}-pillared montmorillonite and Al_{13}-pillared saponite, *J. Phys. Chem. B.*, **103**, 2897 (1999).

62. R.P.T. Janssen, M.G.M. Bruggenwert and W.H. van Riemsdijk, Zinc ion adsorption on montmorillonite–Al hydroxide polymer systems, *Eur. J. Soil Sci.*, **54**, 347 (2003).

63. R.P.T. Janssen, M.G.M. Bruggenwert, G. van Dijk and W.H. van Riemsdijk, Lead ion adsorption on montmorillonite–Al hydroxide polymer systems, *Eur. J. Soil Sci.*, **58**, 1136 (2007).

64. J.Z. He, A.D. Cristofaro and A. Violante, Comparison of adsorption of phosphate, tartrate, and oxalate on hydroxyl aluminum montmorillonite complexes, *Clays Clay Miner.*, **47**, 226 (1999).

65. V. Lenoble, O. Bouras, V. Deluchat, B. Serpaud and J.C. Bollinger, Arsenic adsorption onto pillared clays and iron oxides, *J. Colloid Interface Sci.*, **255**, 52 (2002).

66. K. Kasama, Y. Watanabe, H. Yamada and T. Murakami, Sorption of phosphates on Al-pillared smectites and mica at acidic to neutral pH, *Appl. Clay Sci.*, **25**, 167 (2004).

67.   D. Peak, U.K. Saha and P.M. Huang, Selenite adsorption mechanisms on pure and coated montmorillonite: an EXAFS and XANES spectroscopic study, *Soil Sci. Soc. Am. J.*, **70**, 192 (2006).

68.   L. Yang, Y. Xu, H. Yu, X. Xin, Q. Wei and B. Du, Adsorption of phosphate from aqueous solution by hydroxy-aluminum, hydroxy-iron and hydroxy-iron–aluminum pillared bentonites, *J. Hazard. Mater.*, **179**, 244 (2010).

69.   H. Wang, T. Wu, J. Chen, Q. Zheng, C. He and Y. Zhao, Sorption of Se (IV) on Fe- and Al-modified bentonite, *J. Radioanal. Nucl. Ch.*, **303**, 107 (2015).

70.   M.F. Hou, C.X. Ma, W.D. Zhang, X.Y. Tang, Y.N. Fan and H.F. Wan, Removal of rhodamine B using iron-pillared bentonite, *J. Hazard. Mater.*, **186**, 1118 (2011).

71.   M. Hou, Y. Lv, X. Tang, C. Liu and X. Liang, Adsorption of Neutral Red by iron-pillared bentonite, Advances in Energy Science and Equipment Engineering – Zhou, Patty & Chen (Eds) © 2015 Taylor & Francis Group, London, ISBN 978-1-138-02867-8. Pp 1507–1512.

72.   F. Zahaf, N. Dali, R. Marouf and F. Ouadjenia, Removal of a textile dye by pillared clay, *IJCEE.*, **6**, 11 (2015).

73.   Y. Hao, L. Yan, H. Yu, K. Yang, S. Yu, R. Shan and B. Du, Comparative study on adsorption of basic and acid dyes by hydroxy-aluminum pillared bentonite, *J. Mol. Liq.*, **199**, 202 (2014).

74.   A. Gil, F.C.C. Assis, S. Albeniz and S.A. Korili, Removal of dyes from wastewaters by adsorption on pillared clays, *Chem. Eng. J.*, **168**, 1032 (2011).

75.   F.C.C. Assis, S. Albeniz, A. Gil, S.A. Korili, R. Trujillano, M.A. Vicente, L. Marçal, M. Saltarelli and K.J. Ciuffi, Removal of organic pollutants from industrial wastewater: performance evaluation of inorganic adsorbents based on pillared clays, *Desalin Water Treat.*, **39**, 316 (2012).

76.   H. Khalaf, O. Bouras and V. Perrichon, Synthesis and characterization of Al-pillared and cationic surfactant modified Al-pillared Algerian bentonite, *Microporous. Mater.*, **8**, 141 (1997).

77.   G. Wang, X. Su, Y. Hua, S. Ma, Y. Wang, X. Xue, Q. Tao and S. Komarneni, Kinetics and thermodynamic analysis of the adsorption of hydroxy-Al cations by montmorillonite, *Appl Clay Sci.*, **129**, 79 (2016).

78.   G. Wang, Y. Hua, X. Su, S. Komarneni, S. Ma and Y. Wang, Cr (VI) adsorption by montmorillonite nanocomposites, *Appl Clay Sci.*, **124-125**, 111 (2016).

79.   R. Horvath and K. J. Kowazoe, Method for the calculation of effective pore size distribution in molecular sieve carbon, *Chem. Eng. Jpn.*, **16**, 470 (1983).

80.   P. Tepmatee and P. Siriphannon, Effect of preparation method on structure and adsorption capacity of aluminum pillared montmorillonite, *Mater Res Bull.*, **48**, 4856 (2013).

81.   L. Ma, J. Zhu, H. He, Q. Tao, R. Zhu, W. Shen and B.K.G. Theng, Al_{13}-pillared montmorillonite modified by cationic and zwitterionic surfactants: A comparative study, *Appl Clay Sci.*, **101**, 327 (2014).

82.   W. Tan, Y.H. Zhang, Y.S. Szeto and L.B. Liao, A novel method to prepare chitosan/montmorillonite nanocomposites in the presence of hydroxy-aluminum oligomeric cations, *Compos. Sci. Technol.*, **68**, 2917 (2008).

83.   Z. Qin, P. Yuanb, S. Yang, D. Liu, H. He and J. Zhu, Silylation of Al_{13}-intercalated montmorillonite with trimethylchlorosilane and their adsorption for Orange II, *Appl Clay Sci.*, **99**, 229 (2014).

84.   M.G. Nijkamp, J.E.M.J. Raaymakers, A.J. van Dillen and K.P. de Jong, Hydrogen storage using physisorption-materials demands, *Appl. Phys. A.*, **72**, 619 (2001).

85.   H.L. Wang, Q.M. Gao and J. Hu, High hydrogen storage capacity of porous carbons prepared by using activated carbon, *J. Am. Chem. Soc.*, **131**, 7016 (2009).

86.   M.J. Martinez-Oritz, G. Fetter, J.M. Dominguez, J.A. Melo-Banda and R. Ramos-Gomez, Catalytic hydrotreating of heavy vacuum gas oil on Al- and Ti-pillared clays prepared by conventional and microwave irradiation methods, *Microporous Mesoporous Mater.*, **58**, 73 (2003).

87.   F. Kooli, Porous clay heterostructures (PCHs) from Al_{13}-intercalated and Al_{13}-pillared montmorillonites: Properties and heptanes hydro-isomerization catalytic activity, *Microporous and Mesoporous Mater.*, **184**, 184 (2014).

88.   S. Brunauer, L. S. Deming, W. E. Deming and E. Teller, On a Theory of the van der Waals Adsorption of Gases, *J. Am. Chem. Soc.*, **62**, 1723 (1940).

89.   K. S. W. Sing, D. H. Everett, R. A. W. Haul, L. Moscou, R. A. Pierotti, J. Rouquerol and T. Siemieniewska, Reporting physisorption data for gas/solid systems with special reference to the determination of surface area and porosity, *Pure. Appl. Chem.*, **57**, 603 (1985).

90.   K. Bukka, J.D. Miller and J. Shabtai, FTIR study of deuterated montmorillonite: structural

features relevant to pillared clay stability, *Clays Clay Miner.*, **40**, 92 (1992).

91. A. Gil, M.A. Vicente and S.A. Korili, Effect of the Si/Al ratio on the structure and surface properties of silica-alumina-pillared clays, *J. Catal.*, **229**, 119 (2005).

92. K. Chinoune, K. Bentale, Z. Bouberka, A. Nadim and U. Maschke, Adsorption of reactive dyes from aqueous solution by dirty bentonite, *Appl. Clay Sci.*, **123**, 64 (2016).

93. R. Elmoubarki, F.Z. Mahjoubi, H. Tounsadi, J. Moustadraf, M. Abdennouri, A. Zouhri, A. ElAlban and N. Barka, Adsorption of textile dyes on raw and decanted Moroccan clays: kinetics, equilibrium and thermodynamics, *Water Resour. Ind.*, **9**, 16 (2015).

94. M. Fayazi, D. Afzali, M.A. Taher, A. Mostafavi and V.K. Gupta, Removal of Safranin dye from aqueous solution using magnetic mesoporous clay: optimization study, *J. Mol. Liq.*, **212**, 675 (2015).

95. S.C.R Santos and R.A.R. Boaventura, Adsorption of cationic and anionic azo dyes on sepiolite clay: equilibrium and kinetic studies in batch mode, *J. Environ. Chem. Eng.*, **4**, 1473 (2016).

96. S. Lagergren, Zur theorie der sogenannten adsorption geloster stoffe, Kungliga Svenska Vetenskapsakademiens. *Handlingar.*, **24**, 1 (1898).

97. Y.S. Ho and G. McKay, Kinetic models for the sorption of dye from aqueous solution by wood, *Trans IChemE part B.*, **76**, 183 (1998).

98. Y.S. Ho and G. McKay, Pseudo-second order model for sorption process, *Process Biochem.*, **34**, 451 (1999).

99. S. Fan, Y. Wang, Z. Wang, J. Tang, J. Tang and X. Li, Removal of methylene blue from aqueous solution by sewage sludge-derived biochar: Adsorption kinetics, equilibrium, thermodynamics and mechanism, *J. Environ. Chem. Eng.*, **5**, 601 (2017).

100. X. P. Luo , S. Y. Fu , Y. M. Du , J. Z. Guo and B. Li, Adsorption of methylene blue and malachite green from aqueous solution by sulfonic acid group modified MIL-101, *Microporous and Mesoporous Mater.*, **237**, 268 (2017).

101. Q. Zhou, Q. Gao, W. Luo, C. Yan, Z. Ja and P. Duan, One-step synthesis of amino-functionalized attapulgite clay nanoparticles adsorbent by hydrothermal carbonization of chitosan for removal of methylene blue from wastewater, *Colloid Surf A: Physicochem. Eng. Aspects.*, **470**, 248 (2015).

102. Y. Liu , Y. Kang , B. Mu and A. Wang, Attapulgite/bentonite interactions for methylene blue adsorption characteristics from aqueous solution, *Chem. Eng. J.*, **237**, 403 (2014).

103. J. Chang, J. Ma, Q. Ma, D. Zhang, N. Qiao, M. Hu and H. Ma, Adsorption of methylene blue onto Fe_3O_4/activated montmorillonite nanocomposite, *Appl Clay Sci.*, **119**, 132 (2016).

104. A. K. Kushwaha, N. Gupta and M.C. Chattopadhyaya, Removal of cationic methylene blue and malachite green dyes from aqueous solution by waste materials of Daucus carota, *J. Saudi Chem. Soc.*, **18**, 200 (2014).

105. A. Benhouria, Md. Azharul Islam, H. Zaghouane-Boudiaf, M. Boutahala and B.H. Hameed, Calcium alginate–bentonite–activated carbon composite beads as highly effective adsorbent for methylene blue, *Chem. Eng. J.*, **270**, 621 (2015).

106. L. Cottet, C.A.P. Almeida, N. Naidek, M.F. Viante, M.C. Lopes and N.A. Debacher, Adsorption characteristics of montmorillonite clay modified with iron oxide with respect to methylene blue in aqueous media, *Appl Clay Sci.*, **95**, 25 (2014).

107. Z. Zhang, W. Wang and A. Wang, Highly effective removal of Methylene Blue using functionalized attapulgite via hydrothermal process, *J Environ sci.*, **33**, 106 (2015).

108. Z. Lou, Z. Zhou,W. Zhanga, X. Zhang, X. Hu, P. Liu and H. Zhang, Magnetized bentonite by Fe_3O_4 nanoparticles treated as adsorbent for methylene blue removal from: Synthesis, characterization, mechanism, kinetics and regeneration, *J Taiwan Inst Chem Eng.*, **49**, 199 (2015).

109. S.C.R. Santos, A.F.M. Oliveira and R.A.R. Boaventura, Bentonitic clay as adsorbent for the decolourisation of dyehouse effluents. *J. Clean. Prod.*, **126**, 667 (2016).

110. A. Al-Futaisi, A. Jamrah and R. Ai-Hanai, Aspects of cationic dye molecule adsorption to palygorskite. *Desalination.*, **214**, 327 (2007).

111. M. Rouliaand A.A. Vassiliadis, Sorption characterization of a cationic dye retained by clays and perlite. *Microporous Mesoporous. Mater.*, **116**, 732 (2008).

112. M.T. Yagub, T.K. Sen, S. Afroze and H.M. Ang, Dye and its removal from aqueous solution by adsorption: a review, *Adv. Colloid Interface Sci.*, **209**, 172 (2014).

113. W.A. Khanday, F. Marrakchi, M. Asif and B.H. Hameed, Mesoporous zeolite–activated carbon composite from oil palm ash as an effective adsorbent for methylene blue, *J Taiwan Inst Chem Eng.*, **70**, 32 (2017).

114. M. Auta and B.H. Hameed, Modified mesoporous clay adsorbent for adsorption isotherm and kinetics of methylene blue, *Chem. Eng. J.*, **198–199**, 219 (2012).

115. Z. Shu, T. Li, J. Zhou, Y. Chen, D. Yu and Y. Wang, Template-free preparation of mesoporous silica and alumina from natural kaolinite and their application in methylene blue adsorption, *Appl Clay Sci.*, **102**, 33 (2014).

116. G.K. Sarma, S.S. Gupta and K.G. Bhattacharyya, Adsorption of Crystal violet on raw and acid-treated montmorillonite, K10, in aqueous suspension, *J. Environ. Manage.*, **171**, 1 (2016).

117. S. Debnath and U.C. Ghosh, Nanostructured hydrous titanium (IV) oxide:Synthesis: characterization and Ni(II) adsorption behavior, *Chem. Eng. J.*, **152**, 480 (2009).

118. I. Langmuir, The constitution and fundamental properties of solids and liquids, *J. Am. Chem. Soc.*, **38**, 2221 (1916).

119. H.M.F. Freundlich, Uber die adsorption in Losungen, *Z. Phys. Chem.*, **57**, 385 (1906).

120. M.J. Temkin and V. Pyzhev, Recent modifications to Langmuir isotherms, *Acta Physiochim URSS.*, **12**, 217 (1940).

121. I. Chaari, B. Moussi and F. Jamoussi, Interactions of the dye, C.I. direct orange 34 with natural clay, *J. Alloys Compd.*, **647**, 720 (2015).

122. L. Mouni, L. Belkhiri, J.C. Bollinger, A. Bouzaza, A. Assadi, A. Tirri, F. Dahmoune, K. Madani and H. Remini, Removal of Methylene Blue from aqueous solutions by adsorption on Kaolin: Kinetic and equilibrium studies, *Appl Clay Sci.*, **153**, 38 (2018).

123. D. Ghosh and K.G. Bhattacharyya, Adsorption of methylene blue on kaolinite, *Appl. Clay Sci.*, **20**, 295 (2002).

124. M. Doğan, Y. Özdemir and M. Alkan, Adsorption kinetics and mechanism of cationic methyl violet and methylene blue dyes onto sepiolite, *Dyes Pigm.*, **75**, 701 (2007).

125. A. Rodríguez, G. Ovejero, M. Mestanza and J. García, Removal of dyes from wastewaters by adsorption on sepiolite and pansil, *Ind. Eng. Chem. Res.*, **49**, 3207 (2010).

126. A. Gürses, S. Karaca, C. Doğar, R. Bayrak, M. Açıkyıldız and M. Yalçın, Determina-tion of adsorptive properties of clay/water system: methylene blue sorption, *J. Colloid Interface Sci.*, **269**, 310 (2004).

127. C.H. Weng and Y.F. Pan, Adsorption of a cationic dye (methylene blue) onto spent activated clay, *J. Hazard. Mater.*, **144**, 355 (2007).

128. G. Rytwo, Sh. Nir and L.A Margulies, Model for Adsorption of Divalent Organic Cations to Montmorillonite, *J. Colloid Interface Sci.*, **181**, 551 (1996).

129. Y. Bulut and H. Karaer, Adsorption of methylene blue from aqueous solution by crosslinked chitosan/bentonite composite, *J. Dispers. Sci. Technol.*, **36**, 61 (2015).

130. P. Anadao, I.L.R. Pajolli, E.A. Hildebrando and H. Wiebeck, Preparation and characterization of carbon/montmorillonite composites and nanocomposites from waste bleaching sodium montmorillonite clay, *Adv. Powder Technol.*, **25**, 926 (2014).

131. L.H. Ai, Y. Zhou and J. Jiang, Removal of methylene blue from aqueous solution by montmorillonite/$CoFe_2O_4$ composite with magnetic separation performance, *Desalination.*, **266**, 72 (2011).